Supplemental Figure S1

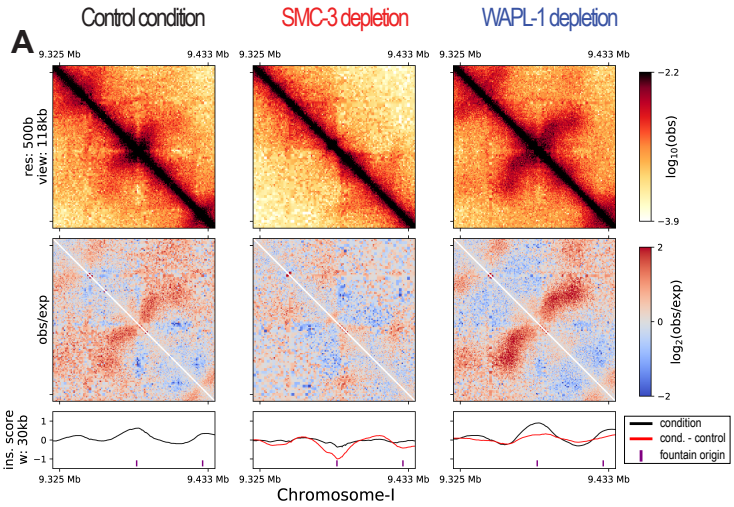

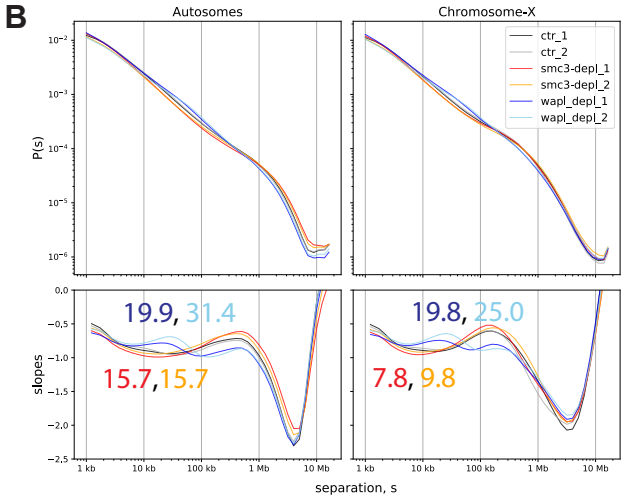

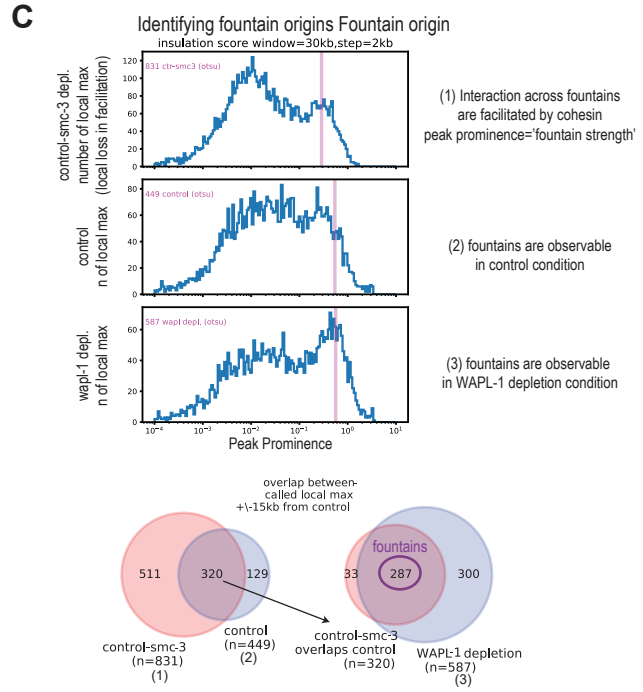

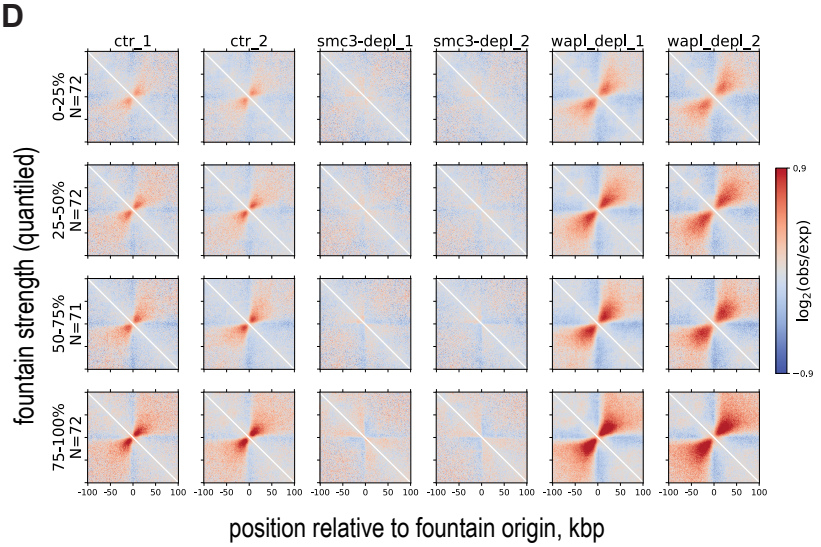

Supplemental Fig S1. Fountain origin identification.

A) Kinked fountain that begins as left-directed and then changes trajectory to the right. B) P(s) and log-derivative plots for three conditions separated by replicates. The numbers indicate inferred loop size of cohesin. C) Top panel: histogram of local maxima with varying degree of peak prominence. We define fountain to have the following properties: (1) interaction across the origin is facilitated by cohesin, (2) fountain is observable in control condition and (3) in WAPL-1 depletion condition. These three conceptual criteria are applied computationally as identifying significant local maxima of (1) insulation scores delta (control condition minus SMC3 depletion condition), (2) insulation scores in control condition, and (3) insulation scores in WAPL-1 depletion condition. The 'fountain strength' corresponds to the peak prominence of insulation scores delta in (1), i.e. degree with which the interaction across the origin is facilitated by cohesin. The significant local maxima are called based on Otsu's method of signal-noise separation indicated by vertical lines on the histogram. Bottom panel: pairwise overlap between significant local maxima called from criteria in A). Due to shift in the maxima occurring from tilt of the fountains, the 'overlap' allows for +/-15kb maximum distance (half of the insulation score window) from the local maxima called by insulation delta (1). We reason that insulation delta (1) provides the most accurate position and strength of the fountains since it corrects for underlying Hi-C structure that is not cohesin dependent. D) On-diagonal pileup of observed-over-expected matrix for each replicate for three conditions is centered at fountain origins divided into quantiles based on the 'fountain strength'.

Supplemental Figure S2

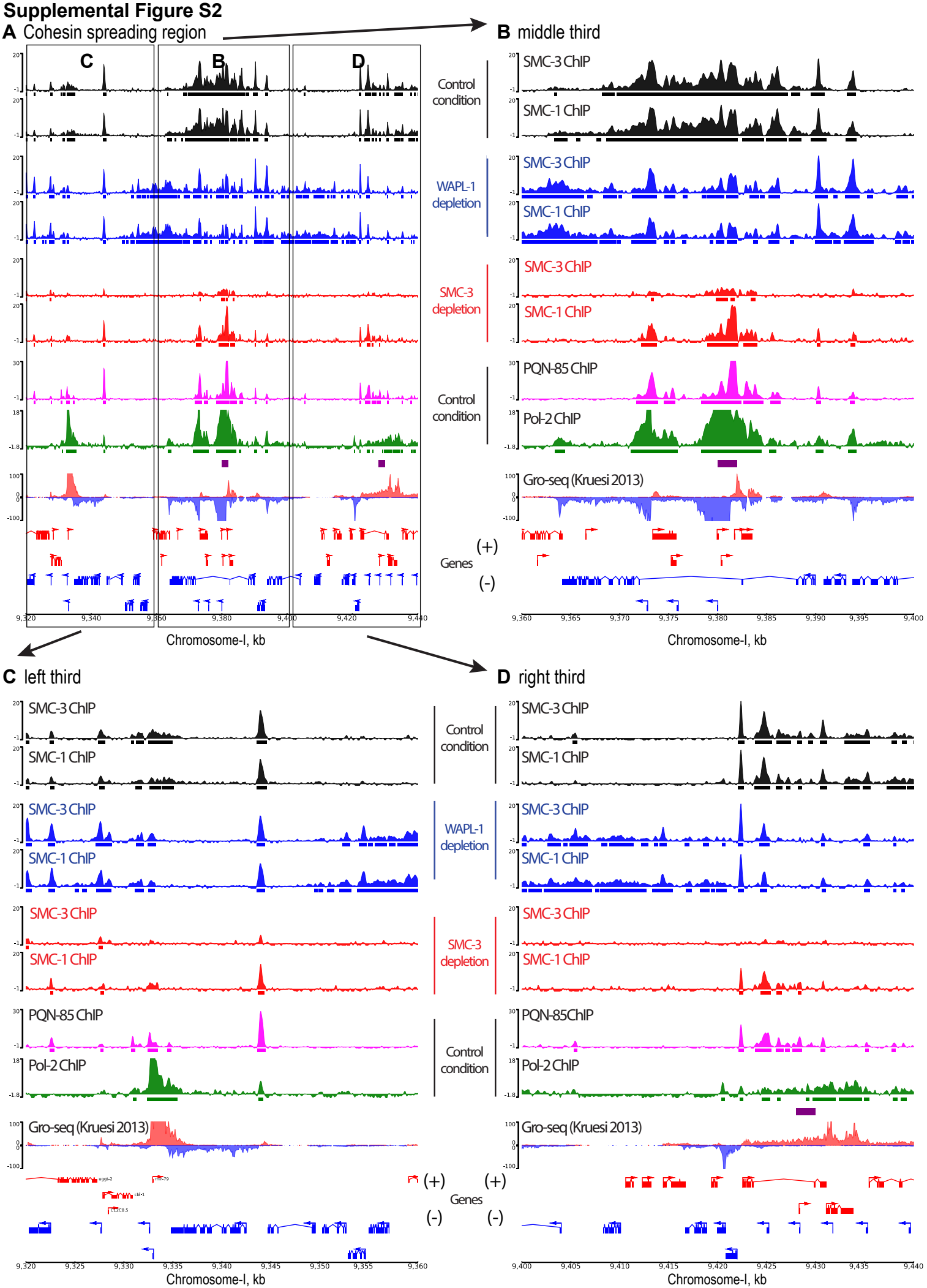

Supplemental Fig S2. Zoom-in of spreading region of cohesin.

A) A region of cohesin binding near fountain origins. The region is subdivided into three segments (B, C, D) to highlight changes in cohesin binding sites upon WAPL-1 depletion. B) Zoom-in of the middle segment C) Zoom-in of the left segment D) Zoom-in of the right segment

Supplemental Figure S3

A

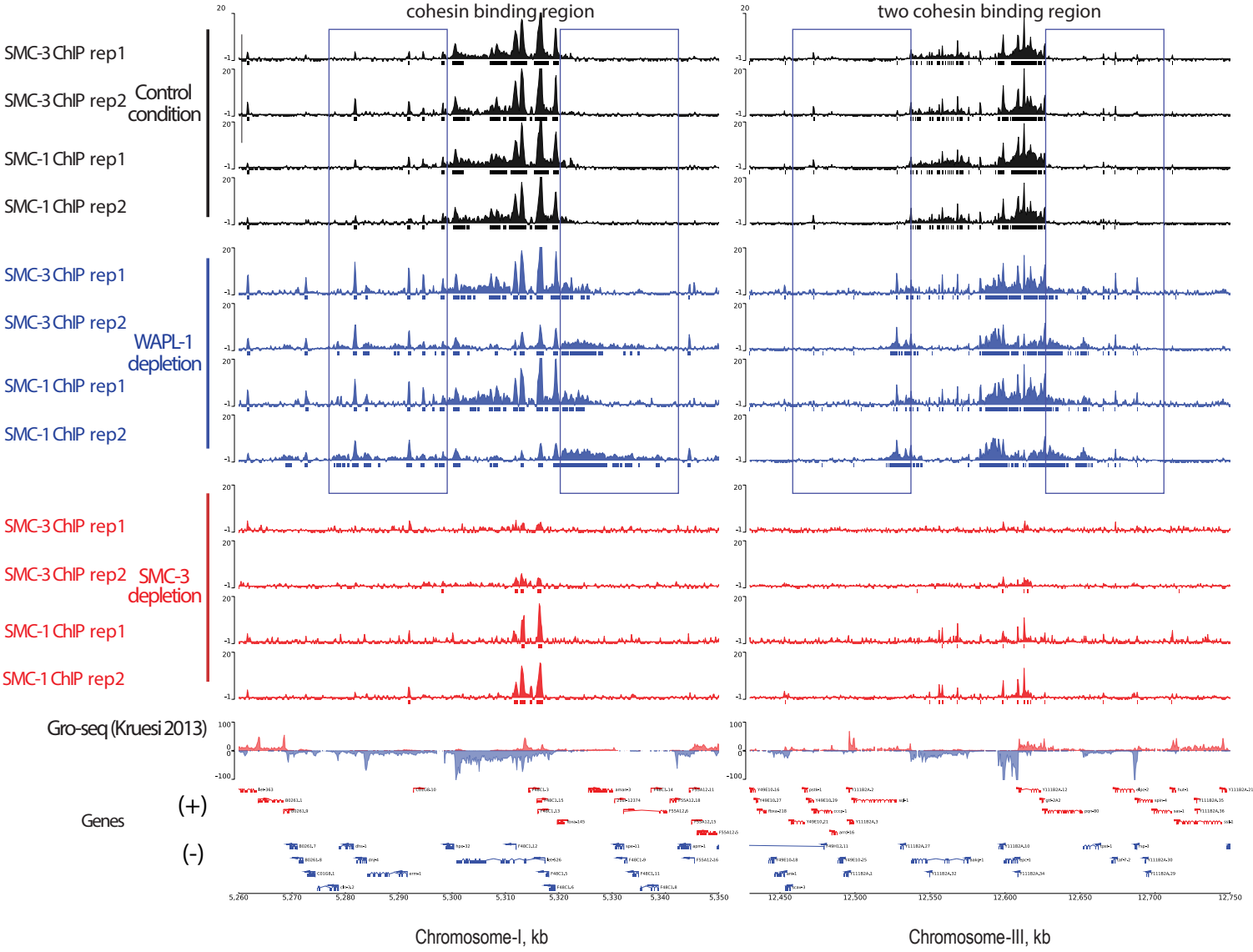

B Residual SMC-1 binding at fountain

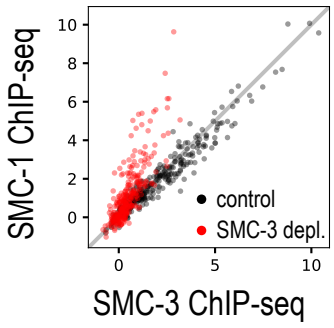

C Cohesin binding at fountain

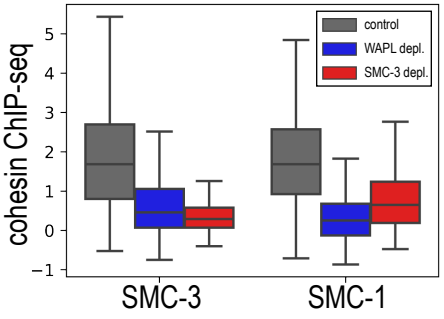

D PQN-85 peaks present in majority of reps

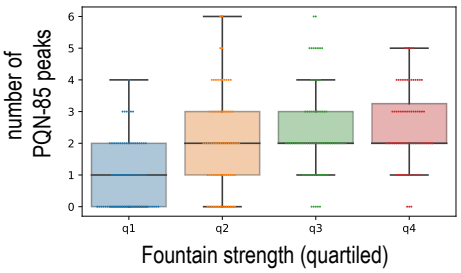

Supplemental Fig S3. Replicates of SMC-1 and SMC-3 ChIP-seq data in control, SMC-3 and WAPL-1 depletion conditions.

A) Genome browser view of input subtracted ChIP replicates corresponding to representative regions. Rectangles are drawn to highlight the outward translocation of cohesin upon WAPL-1 depletion. B) SMC-1 and SMC-3 signal averaged over 6kb region centered at fountain origins. SMC-1 and SMC-3 show similar binding across fountains origins in control condition, but this binding is SMC-1 skewed upon SMC-3 depletion. C) Boxplot of SMC-3 and SMC-1 binding at fountain origins. Input-subtracted ChIP-seq signal over 6kb region centered at fountain origin is averaged. D) Boxplot of fountain strength (divided into quartiles) and the number of PQN-85 summits within 6kb region. Stringent peak summits were used: peaks present both in the merged data as well as in more than half of the replicates.

Supplemental Figure S4

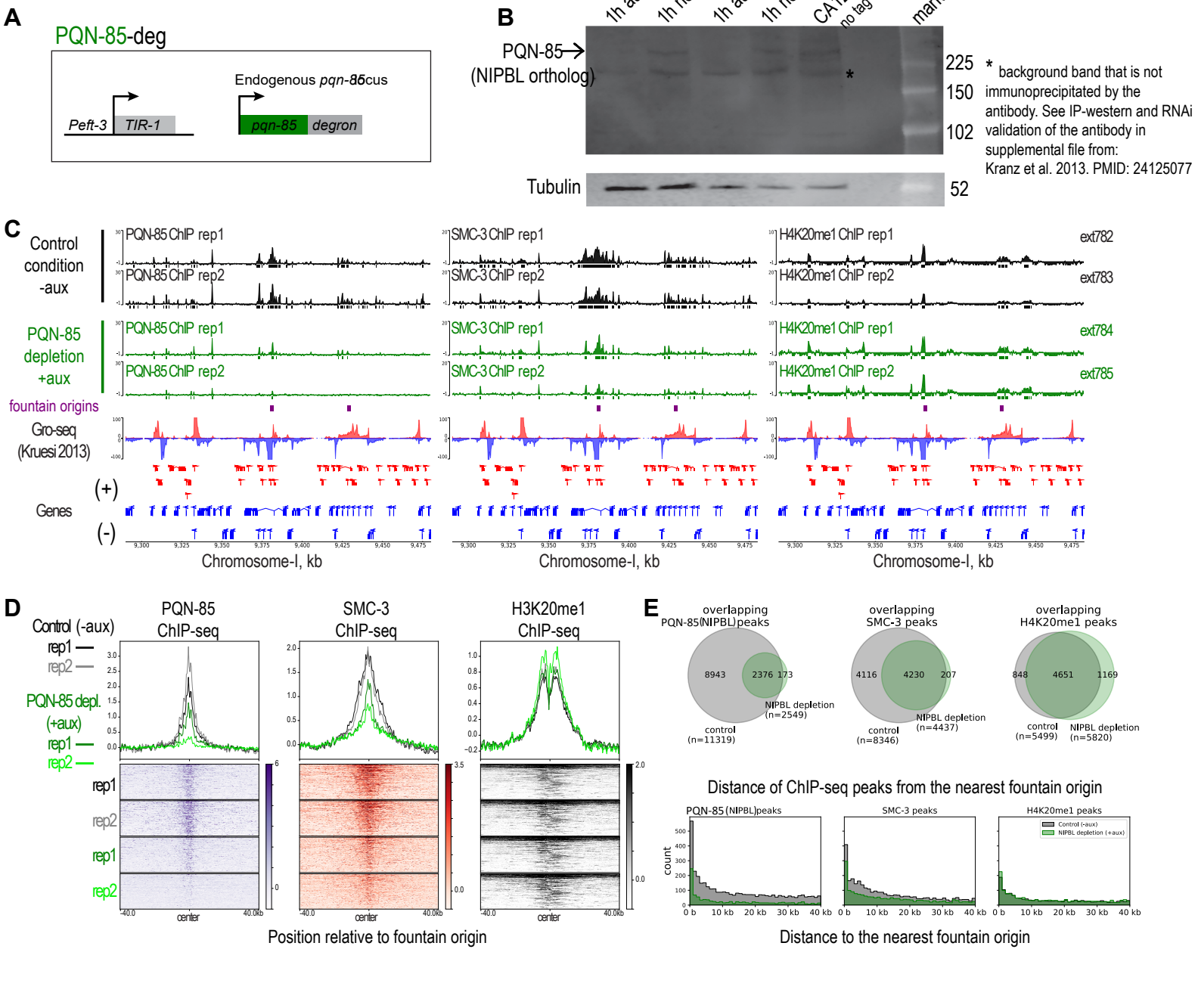

Supplemental Fig S4. PQN-85 depletion.

A) Transgenic strain used in this figure. Exogenously inserted TIR1 is expressed in somatic cells using the eft-3 promoter. Endogenous nipbl (encoded by pqn-85/scc-2 gene) is C-terminally tagged with degron. B) Western blot images of L3 stage worms. CA1200 is tir-1 control lacking degron tag. IP-western from (Kranz et al., 2013) is shown to indicate PQN-85 band size. C) Genome browser view of ChIP replicates for the two conditions with (black) and without auxin (green). Two replicates of PQN-85 (left panel), SMC-3 (center panel), and H4K20me1 (right panel) are shown. The same chromatin extract was used as indicated on the right label to reduce potential technical and biological variability. PQN-85 and SMC-3 show depletion upon auxin treatment. H4K20me1 controls for the quality of the chromatin extract. D) Average profile and heatmap across fountain origins. Upon PQN-85 depletion, both PQN-85 and SMC-3 ChIP-seq signals reduce but not H4K20me1. Note that the saturated signal on top of the heat maps for H4K20me1 is due to X-Chromosome specific enrichment linked to dosage compensation (Albritton & Ercan, 2018). E) Venn-diagram of binding site changes between with and without auxin treatment (top panel). Histogram of binding site distribution relative to the fountain origins (bottom panel).

Supplemental Figure S5

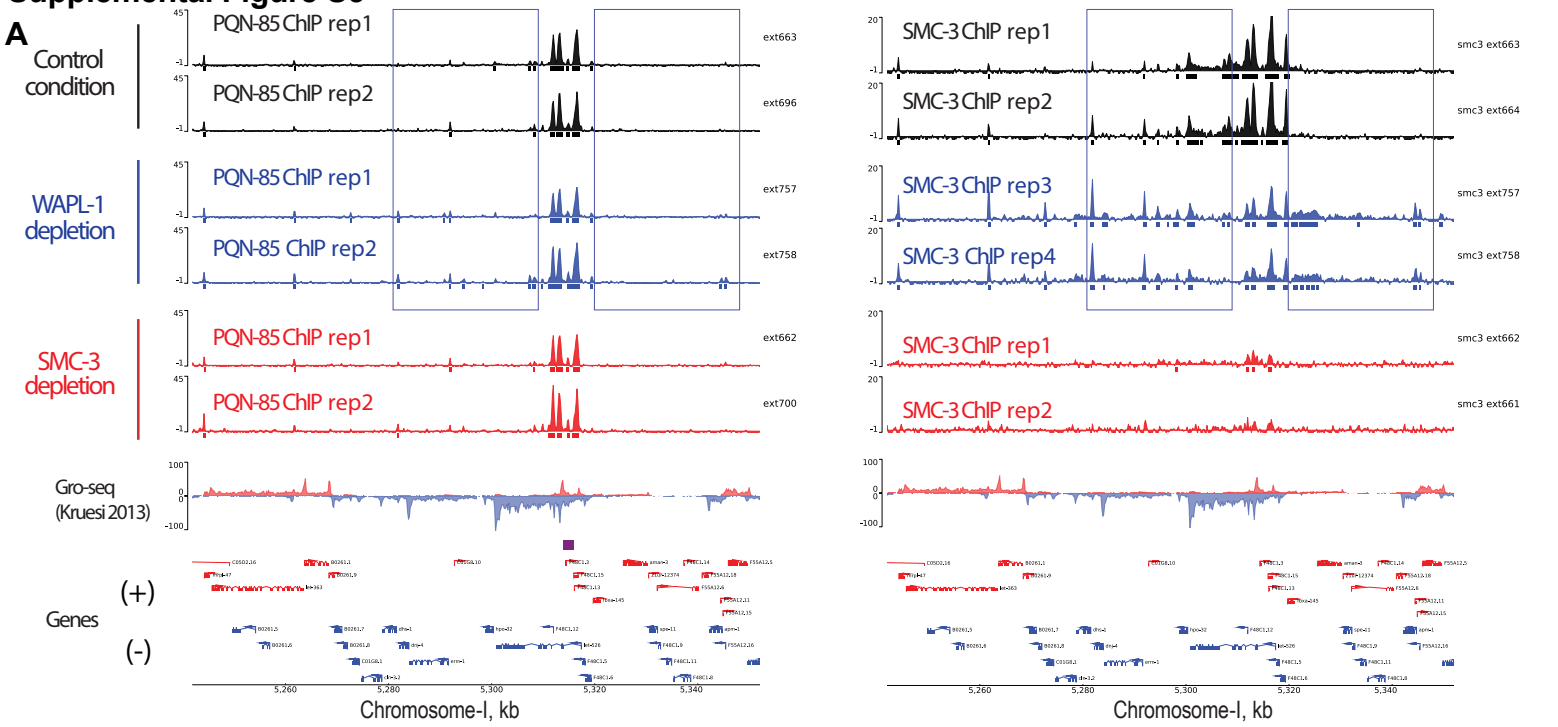

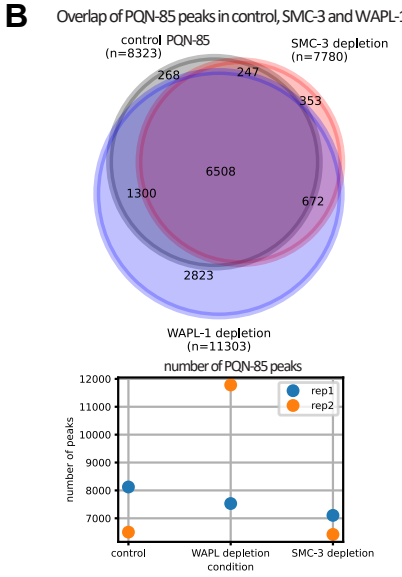

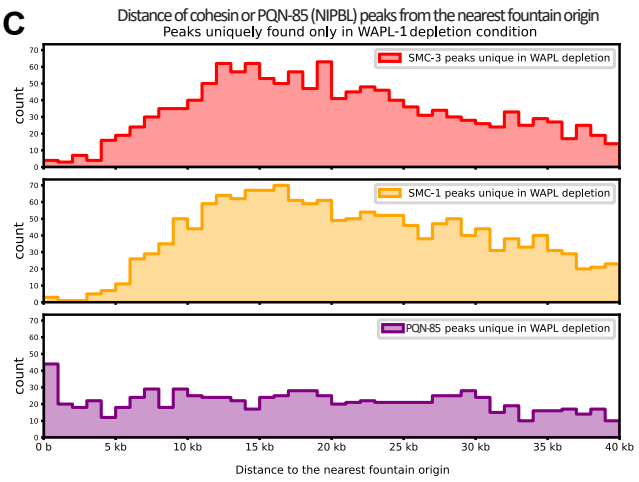

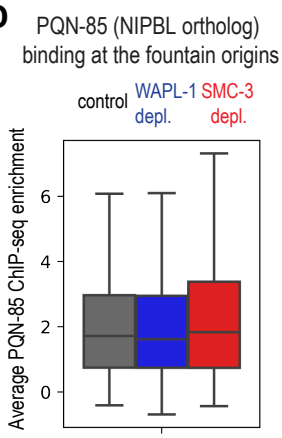

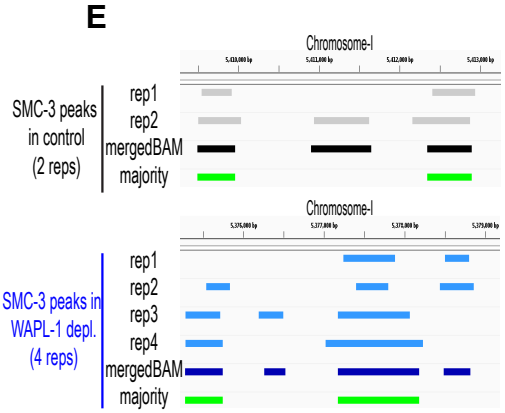

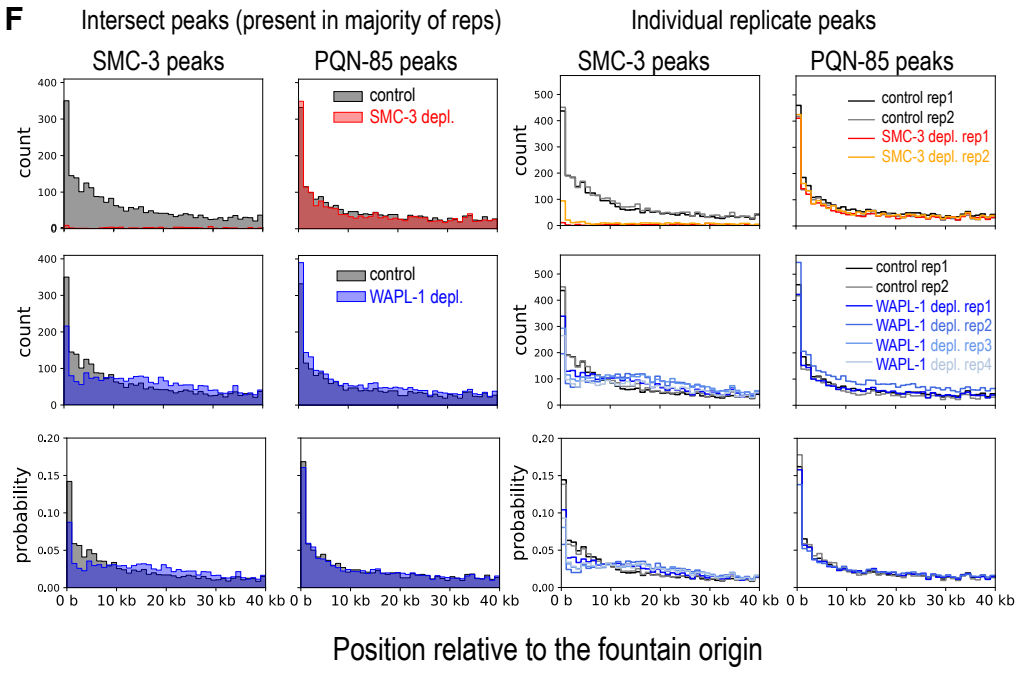

Supplemental Fig S5. Replicates of PQN-85 ChIP-seq data in control, SMC-3 and WAPL-1 depletion conditions.

A) Genome browser view of ChIP replicates. PQN-85 ChIP-seq tracks for the control, WAPL-1, and SMC-3 depletion conditions (left) compared to the SMC-3 ChIP-seq tracks in the same conditions (Right). The ChIP extract identification numbers are provided to compare the effect of WAPL-1 depletion on SMC-3 and PQN-85 in the same ChIP extract and account for biological variability. The rectangles are used to highlight regions outside the cohesin binding regions in control where SMC-3 binding spreads out to in WAPL-1 depletion. The same regions did not show increased PQN-85 binding highlighting that unlike SMC-3, PQN-85 localization is not dependent on WAPL-1. B) Venn-diagram of PQN-85 peaks in three conditions (top). The total number of called peaks for each replicate (bottom). C) Histogram of SMC-3, SMC-1, and PQN-85 ChIP-seq peak distribution with respect to the fountain origins. Only the peaks uniquely found in WAPL-1 depletion are used. Unlike SMC-3 or SMC-1 peaks, the PQN-85 peaks are not enriched away from the fountain origins, thus PQN-85 did not translocate with cohesin upon WAPL-1 depletion. D) Boxplot of PQN-85 binding at fountain origins. Input-subtracted ChIP-seq signal over 6kb region centered at fountain origin is averaged. In contrast to SMC-3 or SMC-1 binding at fountain origins (Supplemental Fig S3C), PQN-85 binding remains intact across perturbation. E) Genome browser view of how “stringent” or “majority” peaks are called by only taking those peaks called from the merged replicate file that are also called from the individual replicates. F) Histogram of distance between SMC-3 or PQN-85 summit and the nearest fountain origin. The three conditions are control (gray), WAPL-1 depletion (blue), and SMC-3 depletion (red). Stringent peak summits were used: peaks present both in the merged data as well as in more than half of the replicates.

Supplemental Figure S6

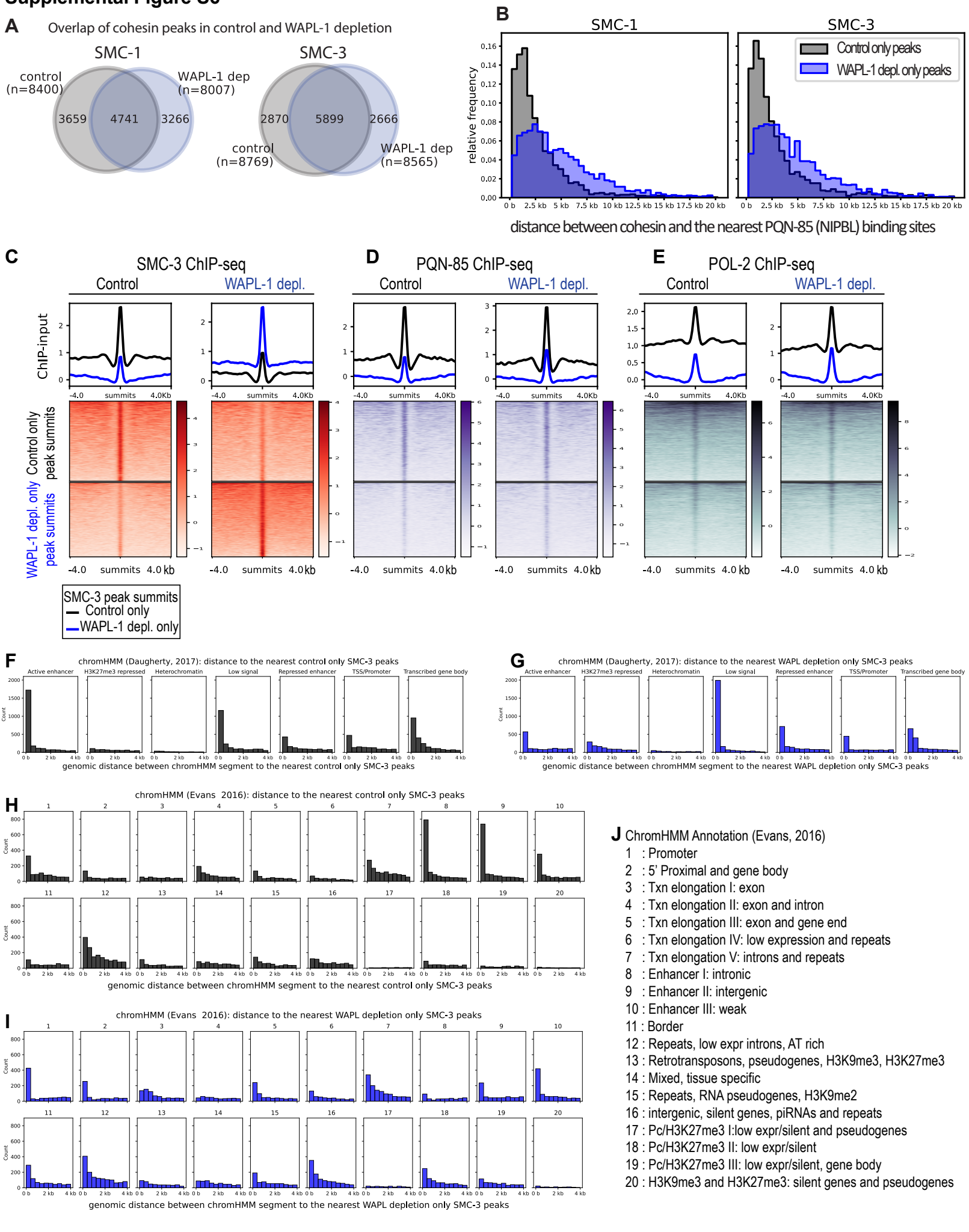

J ChromHMM Annotation (Evans, 2016)

1 : Promoter
2 : 5' Proximal and gene body
3 : Txn elongation I: exon
4 : Txn elongation II: exon and intron
5 : Txn elongation III: exon and gene end
6 : Txn elongation IV: low expression and repeats
7 : Txn elongation V: introns and repeats
8 : Enhancer I: intronic
9 : Enhancer II: intergenic
10 : Enhancer III: weak
11 : Border
12 : Repeats, low expr introns, AT rich
13 : Retrotransposons, pseudogenes, H3K9me3, H3K27me3
14 : Mixed, tissue specific
15 : Repeats, RNA pseudogenes, H3K9me2
16 : intergenic, silent genes, piRNAs and repeats
17 : Pc/H3K27me3 I:low expr/silent and pseudogenes
18 : Pc/H3K27me3 II: low expr/silent
19 : Pc/H3K27me3 III: low expr/silent, gene body
20 : H3K9me3 and H3K27me3: silent genes and pseudogenes

Supplemental Fig S6. Investigation of differential cohesin binding sites.

A) Venn-diagram showing overlap between cohesin binding sites between control and WAPL-1 depletion conditions. B) non-overlapping peaks from A) are used to identify control specific peaks and WAPL-1 depletion specific peaks. Two groups of peaks are used to plot the histogram of distance between cohesin binding site and PQN-85 binding site in the corresponding condition. C) Average profile and heatmap of input subtracted SMC3 ChIP-seq track in control or WAPL-1-depletion conditions for two groups of SMC-3 summits from A). D) Average profile and heatmap of input subtracted PQN-85 ChIP-seq track in control or WAPL-1-depletion conditions for two groups of SMC-3 summits from A). E) Average profile and heatmap of input subtracted Pol II ChIP-seq track in control or WAPL-1-depletion conditions for two groups of SMC-3 summits from A). F) Histogram of distance between control specific SMC-3 summits and annotated ChromHMM in (Daugherty et al., 2017). G) Histogram of distance between WAPL-1 depletion specific SMC-3 summits and annotated ChromHMM in (Daugherty et al., 2017). H) Histogram of distance between control specific SMC-3 summits and annotated ChromHMM in (Evans et al., 2016). I) Histogram of distance between WAPL-1 depletion specific SMC-3 summits and annotated ChromHMM in (Evans et al., 2016). J) Annotation for ChromHMM in H,I. Taken from (Evans et al., 2016).

Supplemental Figure S7

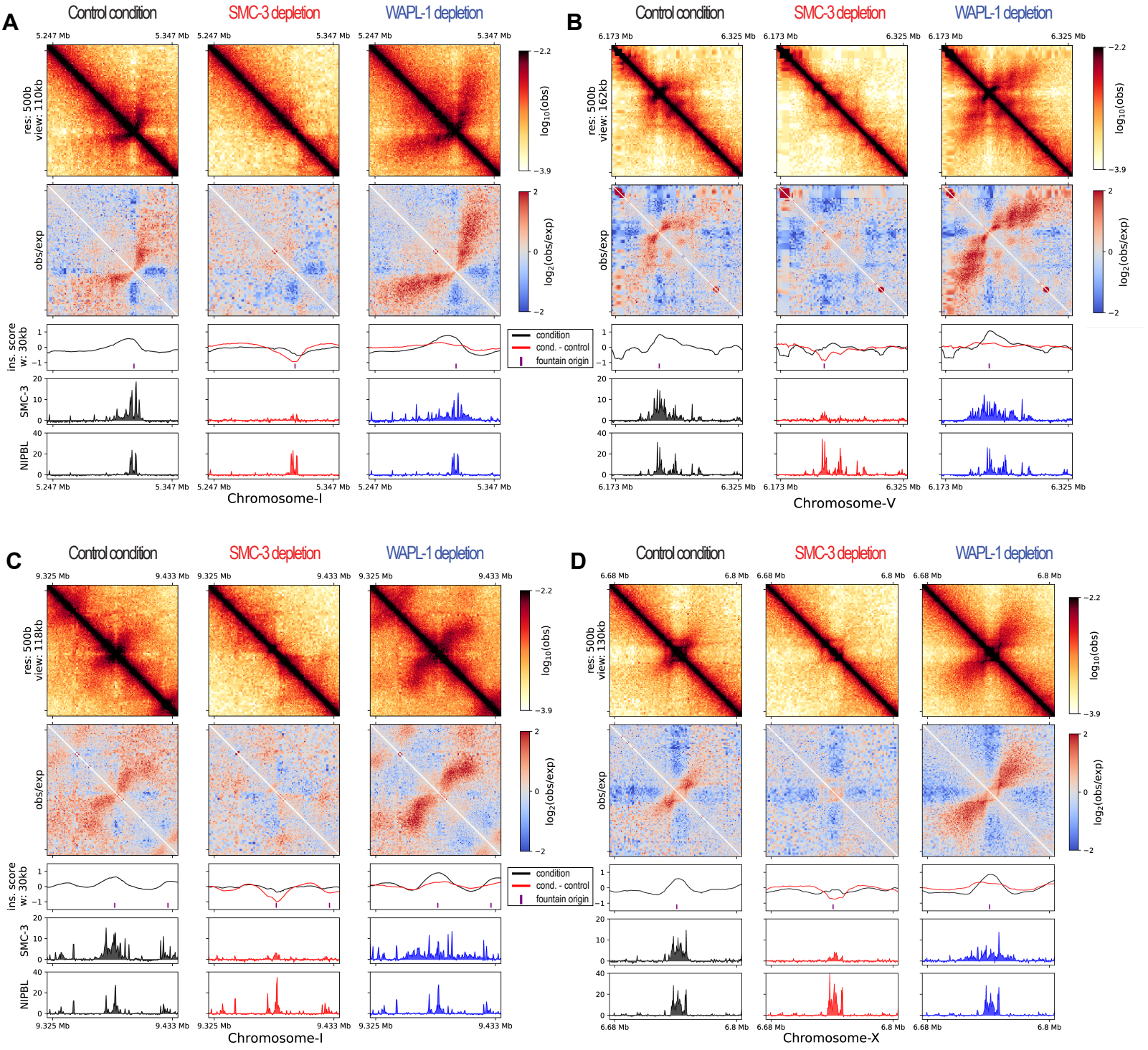

Supplemental Fig S7. Heterogeneity of fountains. Hi-C plots of four regions with insulation scores, SMC-3, and PQN-85 ChIP-seq data.

A) Left-directed fountain. B) Right-directed fountain. C) Kinked fountain that begins as left-directed and then changes trajectory to the right. D) Fountain with embedded stripe pattern.

Supplemental Figure S8

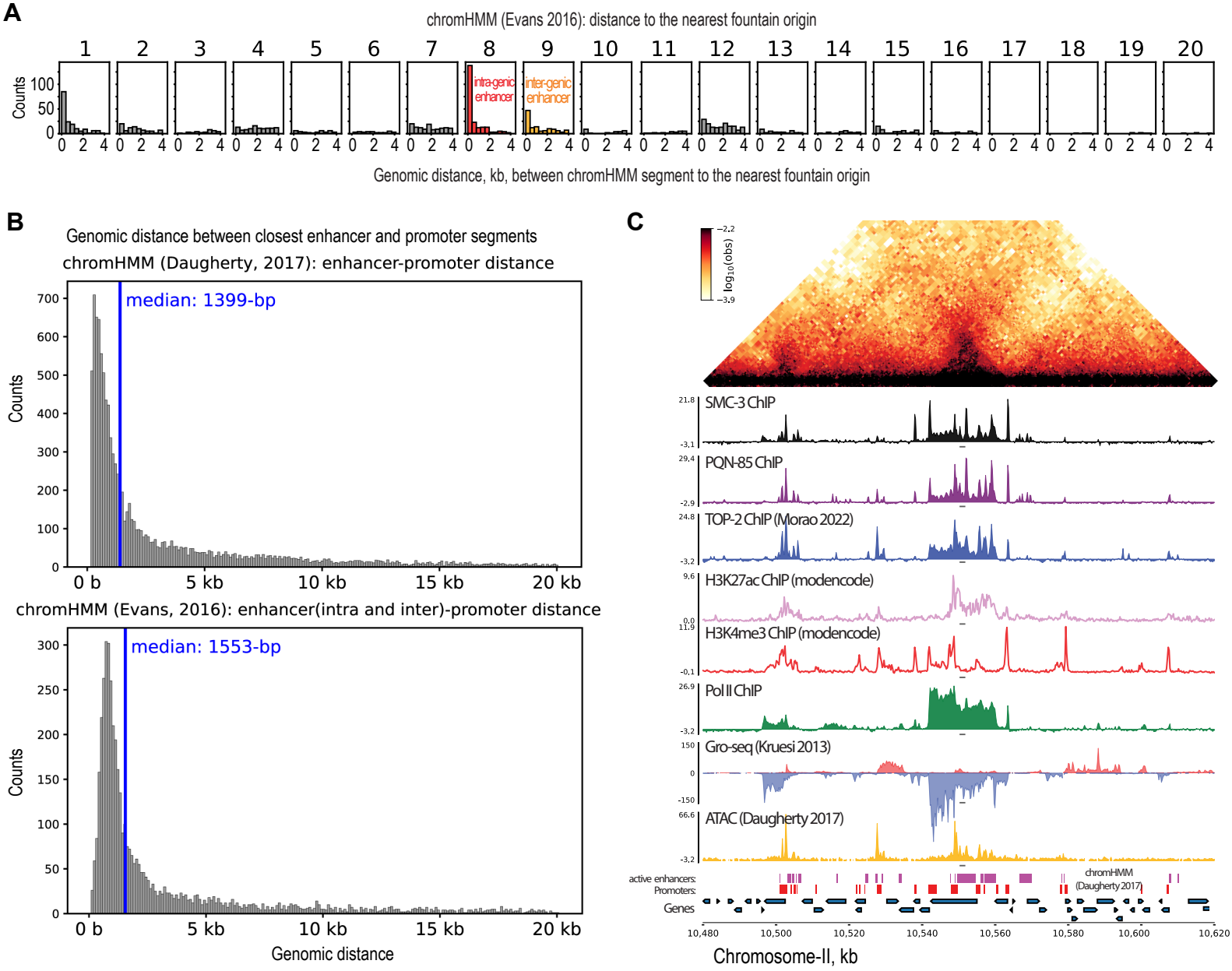

Supplemental Fig S8. Fountains origins coincide with enhancers.

A) Genome browser snapshot of Hi-C and other transcription related features such as topoisomerase-II, H3K27ac, H3K4me3, Pol II, GRO-seq, and ATAC-seq. B) Histogram of distance between enhancer and promoter based on ChromHMM annotations. C) Histogram of 1kb binned genomic distance between identified jet origin in this paper and the annotated regions of ChromHMM (Evans et al., 2016). Segments of ChromHMM are subsampled to match the group containing the fewest number of segments; the shown histogram is an average of histograms generated from ten distinct random subsampling events. The two active enhancer groups are annotated. For detailed description of each group can be found in Supplemental Fig S6J. The annotations are directly taken from the original paper (Evans et al., 2016).

Supplemental Figure S9

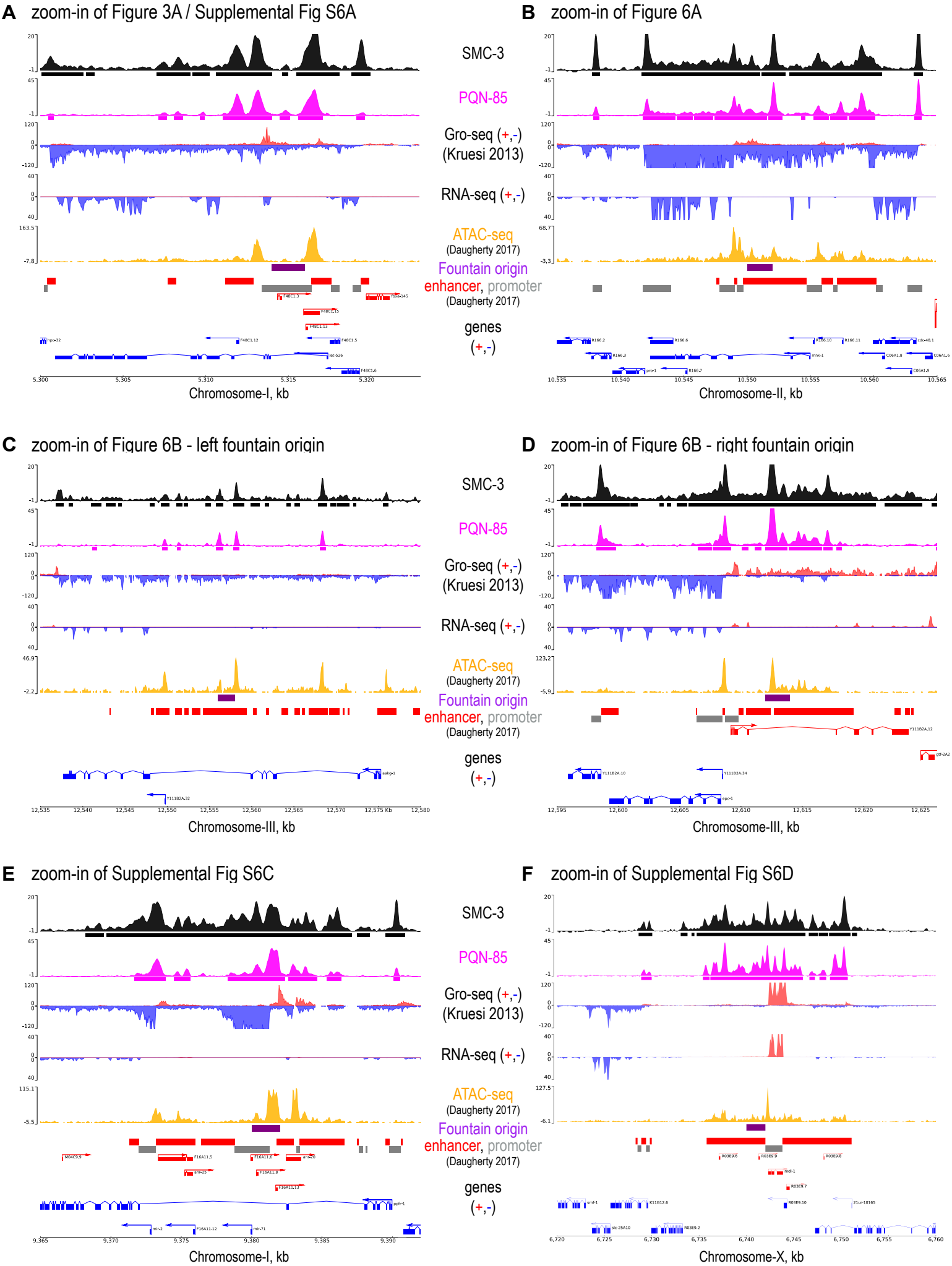

Supplemental Fig S9. Zoom-in of various regions around fountain origins.

The ChIP-seq tracks (SMC-3 and PQN-85) and RNA-seq track are from this study. Other key features such as GRO-seq (Kruesi et al., 2013) and ATAC-seq (Daugherty et al., 2017) are also plotted as well as the ChromHMM from the same study.

Supplemental Figure S10

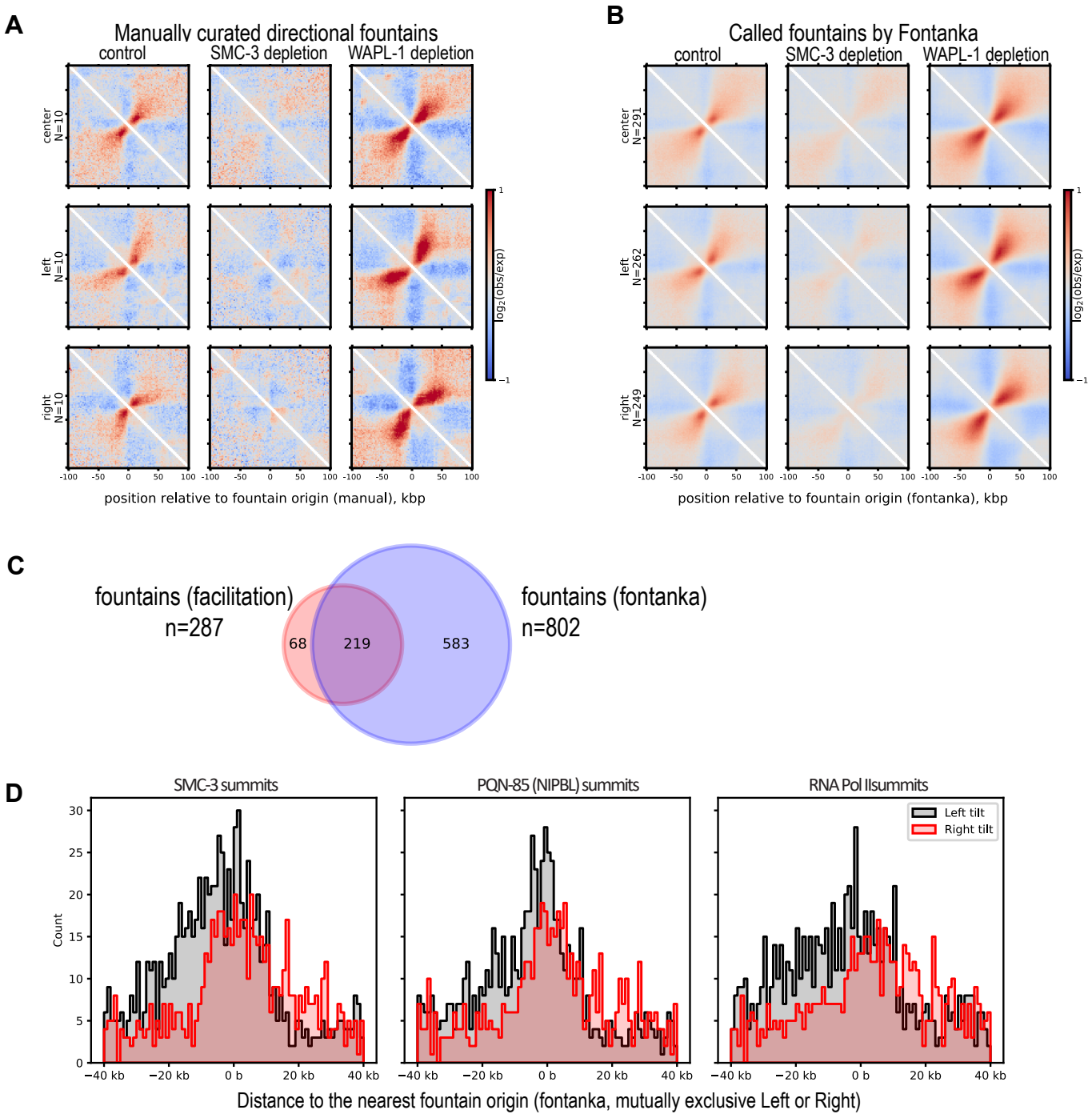

Supplemental Fig S10. Identifying direction specific fountains using the fontanka tool.

A) By manually scanning the genome, fountains are annotated left or right directed based on the orientation. B) Manually selected fountains are used as masks for identifying fountains following the published method (see Methods) (Galitsyna et al., 2023). The identified fountains are plotted for each group. C) Overlap between fountains identified by insulation scores in Supplemental Fig S1 and by fontanka. D) ChIP-seq summit distribution relative to the fontanka identified left and right tilted fountain origins.

Supplemental Figure S11

A

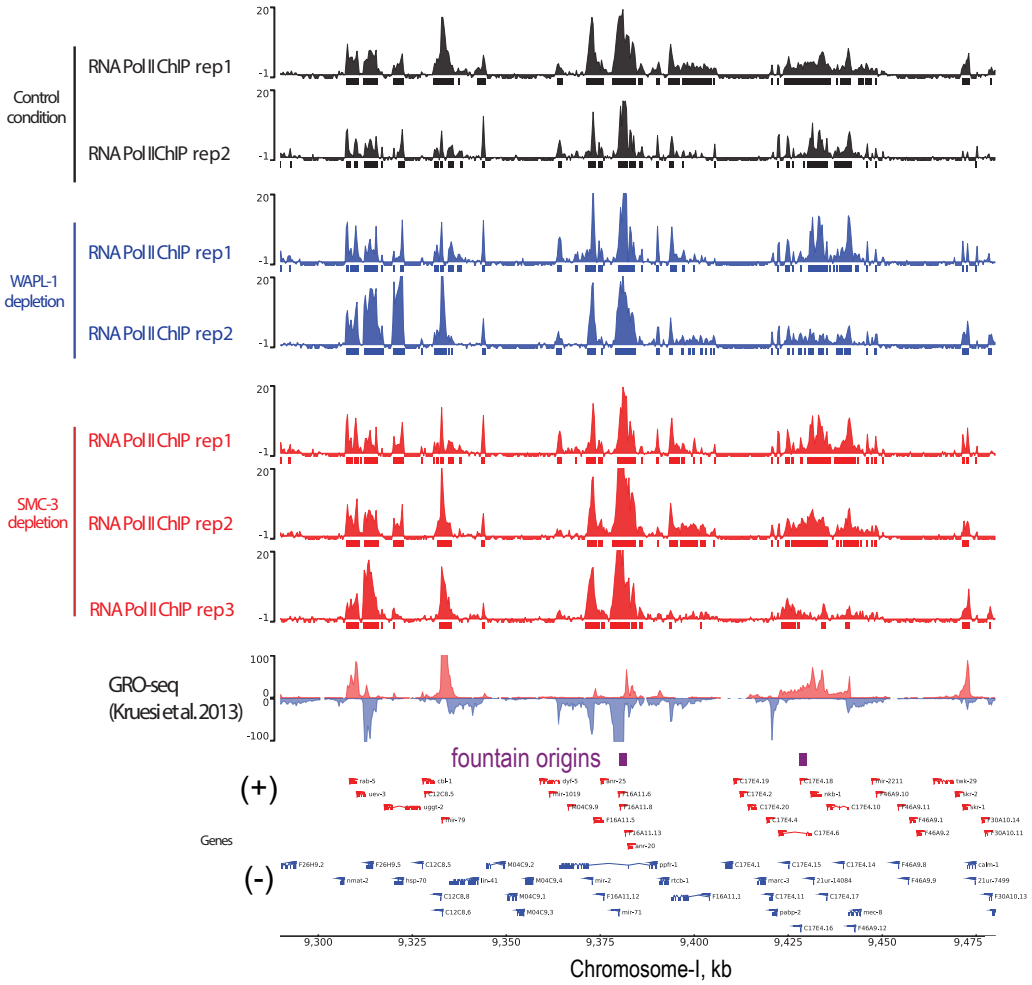

B

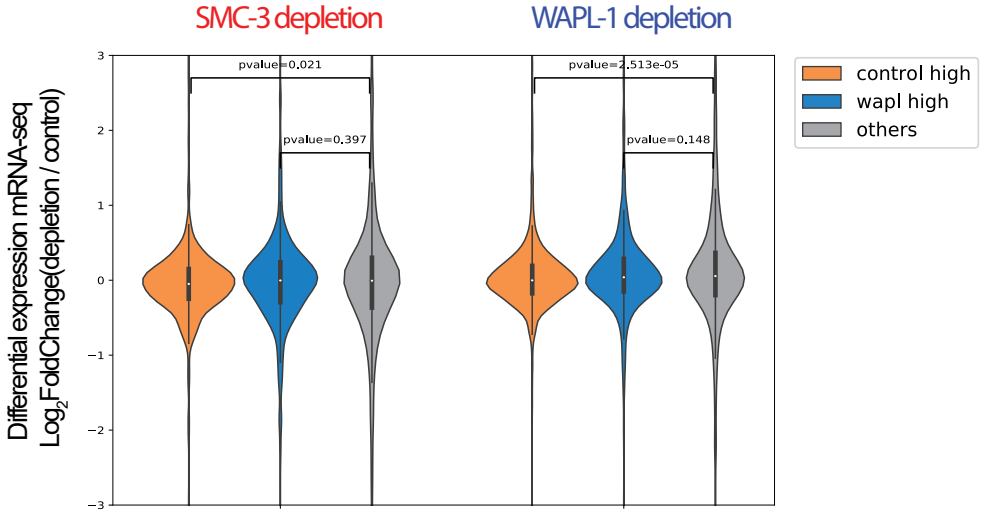

Supplemental Fig S11. Replicates of RNA Pol II ChIP-seq data and mRNA-seq upon 4-hour depletion.

A) RNA Pol II ChIP-seq tracks for the control, WAPL-1, and SMC-3 depletion conditions at an example region in the region. B) Differential expression values (log_2fc from DESeq2) is plotted for three categories of genes upon 4-hour SMC-3 and WAPL-1 depletion. No-tag strain was used as control. Mann-Whitney *U* test was used to generate p-values.

References in supplemental figures

Albritton, S. E., & Ercan, S. (2018). Caenorhabditis elegans Dosage Compensation: Insights into Condensin-Mediated Gene Regulation. *Trends Genet*, *34*(1), 41-53. https://doi.org/10.1016/j.tig.2017.09.010

Daugherty, A. C., Yeo, R. W., Buenrostro, J. D., Greenleaf, W. J., Kundaje, A., & Brunet, A. (2017). Chromatin accessibility dynamics reveal novel functional enhancers in C. elegans. *Genome Res*, *27*(12), 2096-2107. https://doi.org/10.1101/gr.226233.117

Evans, K. J., Huang, N., Stempor, P., Chesney, M. A., Down, T. A., & Ahringer, J. (2016). Stable Caenorhabditis elegans chromatin domains separate broadly expressed and developmentally regulated genes. *Proc Natl Acad Sci U S A*, *113*(45), E7020-E7029. https://doi.org/10.1073/pnas.1608162113

Galitsyna, A., Ulianov, S. V., Bykov, N. S., Veil, M., Gao, M., Perevoschikova, K., Gelfand, M., Razin, S. V., Mirny, L., & Onichtchouk, D. (2023). Extrusion fountains are hallmarks of chromosome organization emerging upon zygotic genome activation. *bioRxiv*. https://doi.org/10.1101/2023.07.15.549120

Kranz, A. L., Jiao, C. Y., Winterkorn, L. H., Albritton, S. E., Kramer, M., & Ercan, S. (2013). Genome-wide analysis of condensin binding in Caenorhabditis elegans. *Genome Biol*, *14*(10), R112. https://doi.org/10.1186/gb-2013-14-10-r112

Kruesi, W. S., Core, L. J., Waters, C. T., Lis, J. T., & Meyer, B. J. (2013). Condensin controls recruitment of RNA polymerase II to achieve nematode X-chromosome dosage compensation. *Elife*, *2*, e00808. https://doi.org/10.7554/eLife.00808